Photoionization spectroscopy of the SiH free radical in the vacuum-ultraviolet range

Ning Lucie Chen, Bérenger Gans, Sebastian Hartweg, Gustavo A Garcia, Séverine Boyé-Péronne, Jean-Christophe Loison

The Journal of Chemical Physics

Photoionization spectroscopy of the SiH free radical in the vacuum-ultraviolet range

Cite as: J. Chem. Phys. **157**, 014303 (2022); https://doi.org/10.1063/5.0094863
Submitted: 06 April 2022 • Accepted: 13 June 2022 • Accepted Manuscript Online: 13 June 2022 • Published Online: 01 July 2022

Ning L. Chen, Bérenger Gans, Sebastian Hartweg, et al.

The Journal of Chemical Physics ARTICLE scitation.org/journal/jcp

Photoionization spectroscopy of the SiH free radical in the vacuum-ultraviolet range

Cite as: J. Chem. Phys. **157**, 014303 (2022); doi: 10.1063/5.0094863
Submitted: 6 April 2022 • Accepted: 13 June 2022 •
Published Online: 1 July 2022

Ning L. Chen,[1] Bérenger Gans,[1] Sebastian Hartweg,[2] Gustavo A. Garcia,[2] Séverine Boyé-Péronne,[1] and Jean-Christophe Loison[3,a)]

AFFILIATIONS

[1] Institut des Sciences Moléculaires d'Orsay, CNRS, Université Paris-Saclay, F-91405 Orsay, France
[2] Synchrotron SOLEIL, L'Orme des Merisiers, St. Aubin, F-91192 Gif sur Yvette, France
[3] Institut des Sciences Moléculaires, CNRS, Université de Bordeaux, F-33400 Talence, France

[a)] **Author to whom correspondence should be addressed:** jean-christophe.loison@cnrs.fr

ABSTRACT

The first measurement of the photoelectron spectrum of the silylidyne free radical, SiH, is reported between 7 and 10.5 eV. Two main photoionizing transitions involving the neutral ground state, $X^+\,^1\Sigma^+ \leftarrow X\,^2\Pi$ and $a^+\,^3\Pi \leftarrow X\,^2\Pi$, are assigned by using *ab initio* calculations. The corresponding adiabatic ionization energies are derived, $IE_{ad}(X^+\,^1\Sigma^+) = 7.934(5)$ eV and $IE_{ad}(a^+\,^3\Pi) = 10.205(5)$ eV, in good agreement with our calculated values and the previous determination by Berkowitz *et al.* [J. Chem. Phys. **86**, 1235 (1987)] from a photoionization mass spectrometric study. The photoion yield of SiH recorded in this work exhibits a dense autoionization landscape similar to that observed in the case of the CH free radical [Gans *et al.*, J. Chem. Phys. **144**, 204307 (2016)].

I. INTRODUCTION

Chemically similar to carbon, silicon is believed to be an element that exists abundantly in interstellar space.[1,2] Even though most silicon is in the form of silicates, the chemistry of the remaining silicon (estimated at around 1% of total silicon[3,4]) is very poorly known.[1] All species containing silicon are, therefore, potentially very interesting to better understand the chemistry of silicon. Unlike the various silicon compounds, such as SiC,[5] SiH_4,[6] SiO,[7–9] SiN,[10,11] SiS,[12] and SiCN,[13] that have been already detected in space, the existence of SiH is still not ascertained albeit for a tentative detection from Orion-KL,[14] several decades after the prediction of its existence in 1978.[15] Although not unambiguously detected in space, SiH and its cation SiH^+ are suspected to be key intermediates in silicon chemistry in the gas phase[1] and also on grains from the hydrogenation of atomic silicon sticking to the grains. The addition reactions of hydrogen atoms are, indeed, omnipresent on the grains.[16]

In the 1980s, Berkowitz *et al.*[17] studied the photoionization of the SiH radical between 1600 and 1200 Å by photoionization mass spectrometry with a wavelength resolution of about 0.8 Å. They used reactions of F atoms with SiH_4 to generate the SiH_n radicals. In their paper, they published the first measurement of the SiH adiabatic ionization energy. For this, they used the rather abrupt onset in the SiH^+ ion yield and located the ionization threshold as approximately the half-rise point to the direct ionization plateau. This led to $IE = 7.91 \pm 0.01$ eV. They also discussed the autoionization processes that strongly affect the SiH^+ ion yield and partly assigned the autoionization features to neutral Rydberg series converging to the first excited electronic state of the cation ($a^+\,^3\Pi$). From this analysis, they inferred an ionization limit for the a^+ state at 10.21 eV.

From the theoretical side, the SiH photoionization has also been investigated, leading to *IE* values of 7.86[18] and 7.93 eV[19] (toward the cation ground state).

In this paper, a radical source similar to the one of Berkowitz *et al.*[17] (i.e., a microwave discharge that generates fluorine atoms coupled to a flow-tube reactor) was employed to efficiently produce *in situ* the radicals from the SiH_4 precursor. Its coupling with a double-imaging photoelectron/photoion coincidence (i^2PEPICO) spectrometer and a synchrotron radiation source allowed us to acquire the ion yield and mass-selected photoelectron spectra for a series of Si_xH_y products. Only the results obtained for the SiH

radical are discussed in this paper. The first measurement of the threshold photoelectron spectrum presented here yields reliable values of ionization energies (*IE*) with an improved accuracy. From our experimental photoionization spectrum, we tentatively progress in the autoionization feature assignments initiated by Berkowitz *et al.*[17]

This paper is organized as follows: In Sec. II, we introduce our experimental and calculation methodologies. In Sec. III, we present our experimental photoelectron and ion yield spectra and we discuss the vibronic structure of SiH^+ and the Rydberg state landscape above the first ionization threshold observed through autoionization processes. Section IV gives the conclusion and perspectives for this work.

II. METHODOLOGIES

A. *Ab initio* calculations

The *ab initio* calculations on the electronic states of SiH and its cation SiH^+ were carried out by using the internally contracted multireference configuration interaction method with Davidson correction (MRCI + Q) with complete active space self-consistent field (CASSCF) wave functions. The CASSCF and MRCI calculations were performed at full valence, namely, with 15 (14 for SiH^+) electrons distributed in 17 orbitals with the 1s, 2s, and 2p orbitals of silicon atom kept doubly occupied and fully optimized. All calculations were performed by using the MOLPRO 2015 package.[20] The main configuration of the two lowest electronic states of SiH and the three lowest electronic states of its cation SiH^+ are given in the following:

$$\begin{aligned}
&\mathrm{SiH}(\mathrm{X}^2\Pi) : (1\sigma)^2(2\sigma)^2(3\sigma)^2(1\pi)^4(4\sigma)^2(5\sigma)^2(2\pi)^1\\
&\text{or } (1s\sigma)^2(2s\sigma)^2(2p\sigma)^2(2p\pi)^4(3s\sigma)^2(3p\sigma)^2(3p\pi)^1,\\
&\mathrm{SiH}(\mathrm{a}^4\Sigma^-) : [\ldots](4\sigma)^2(5\sigma)^1(2\pi)^2,\\
&\mathrm{SiH}^+(\mathrm{X}^{+\,1}\Sigma^+) : [\ldots](4\sigma)^2(5\sigma)^2(2\pi)^0,\\
&\mathrm{SiH}^+(\mathrm{a}^{+\,3}\Pi \text{ and } \mathrm{A}^{+\,1}\Pi) : [\ldots](4\sigma)^2(5\sigma)^1(2\pi)^1.
\end{aligned}$$

For the neutral ground state, the "united-atom" configuration is also given in view of the discussion on autoionization via Rydberg states (see Sec. III B).

The potential energy curves of these five states were computed as a function of the Si–H bond length, R(Si– H), by using the AVnZ (augmented-VnZ) (n = T, Q, 5, and 6) basis sets. Typical plots are shown in Fig. 1. Equilibrium geometries for the $SiH(X^2\Pi)$, $SiH(a^4\Sigma^-)$, $SiH^+(X^{+1}\Sigma^+)$, and $SiH^+(a^{+3}\Pi)$ states were calculated by using the OPTG routine in MOLPRO with the AVnZ (n = T, Q, 5, and 6) basis sets. Anharmonic frequencies were calculated by using the DIATOMIC routine in MOLPRO with the same basis sets, where the potential curves for the $SiH(X^2\Pi)$, $SiH(a^4\Sigma^-)$, $SiH^+(X^{+1}\Sigma^+)$, and SiH^+ $(a^{+3}\Pi)$ states, shown in Fig. 1, were fitted with a polynomial of order 8, allowing the spectroscopic constants to be calculated (ω_e, $\omega_e x_e$, and $\omega_e y_e$). Complete basis set (CBS) extrapolations were carried out by using the AVnZ (n = T, Q, 5, and 6) basis set series. The CASSCF (E_{CASSCF}) and dynamical correlation ($E_{\mathrm{MRCI+Q}} - E_{\mathrm{CASSCF}}$) energies were extrapolated by using the $E_{\mathrm{CASSCF}}(\mathrm{CBS}) + A \times \exp(-Bn)$ and $E_{\mathrm{Corr}}(\mathrm{CBS}) + C \times n^{-3}$ functions, respectively. The vibrational frequencies (ω_e) and equilibrium geometries (R_e) were extrapolated by using the same function as for the dynamical correlation extrapolation. The calculated energies reported in this paper correspond to $E_{\mathrm{CASSCF}}(\mathrm{CBS}) + E_{\mathrm{Corr}}(\mathrm{CBS})$ corrected by the zero-point energy [E(corr ZPE) given in Table I]. All the calculated values are reported and compared with calculated values from the literature[19,21] in Table I.

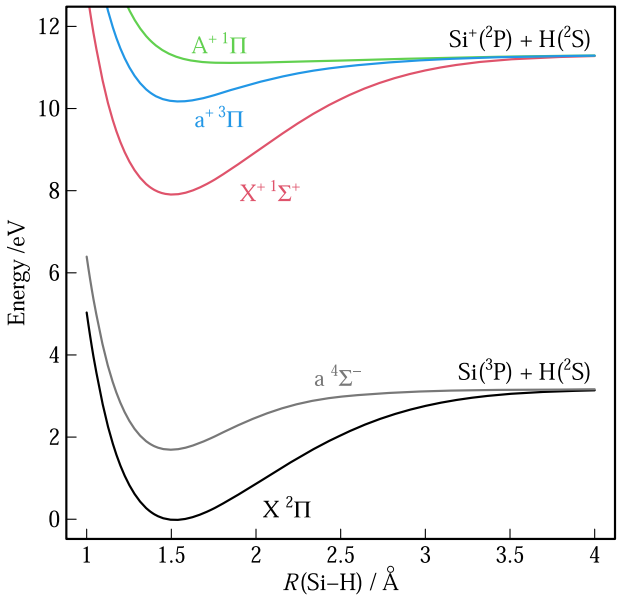

FIG. 1. Calculated potential energy curves (MRCI/AV6Z method) of the ground state $X^2\Pi$ and the first excited electronic state $a^4\Sigma^-$ of neutral SiH, as well as the ground state $X^{+1}\Sigma^+$ and the two lowest excited states $a^{+3}\Pi$ and $A^{+1}\Pi$ of SiH^+ cation. The single-point energies have been calculated every 0.01 Å.

The Franck–Condon (FC) calculations shown in Sec. III A were performed with the PGOPHER[22] and ezFCF[23] software by using the *ab initio* output files (Molden output files calculated with the AVQZ basis set for all states) and neglecting spin. The adiabatic transition energies obtained by the CBS extrapolations corrected from the ZPE were used to fix the energy of the origin bands ($v^+ = 0 \leftarrow v = 0$) of the calculated spectra.

B. Experimental details

The experiments were performed at the SOLEIL French synchrotron facility on the DESIRS beamline[25] and have been described in detail previously.[26,27] SiH_4 (1×10^{13} molecules cm^{-3}) seeded in helium carrier gas (1:1000) was introduced into the flow tube reactor (total pressure of 4×10^{-1} mbar) to react with the F atoms (around 1×10^{13} atoms cm^{-3}) produced upstream by a microwave discharge on F_2. F atoms react with SiH_4 along successive H-atom abstraction reactions to generate a series of SiH_n radicals. By adjusting the experimental conditions such as the concentration of F atom, gas flows, or injector distance, the production of SiH radical was optimized considering the compromise between selectivity and productivity.

TABLE I. Calculated molecular properties of the two lowest electronic states of the neutral and cationic species of SiH free radical. All values from this paper correspond to complete basis set extrapolations (see text for details), except for the anharmonicity constants that are calculated at the AV6Z level of theory. Previous theoretical values from the literature are reported in brackets.

State	E (eV)	E(corr ZPE) (eV)	R_e (Å)	ω_e (cm^{-1})	$\omega_e x_e$ (cm^{-1})	$\omega_e y_e$ (cm^{-1})
$X^2\Pi$	0	0	1.521 (1.5169)[21]	2043.87 (2041.5346)[21]	35.88 (32.9505)[21]	0.07
$a^4\Sigma^-$	1.715 (1.7528)[21]	1.716	1.493 (1.4893)[21]	2059.24 (2069.6140)[21]	57.80 (64.8035)[21]	−1.65
$X^{+1}\Sigma^+$	7.927	7.934 (7.93)[19]	1.505 (1.510)[19]	2154.37 (2153.5)[19] (2155.35)[24]	33.64 (38.9)[19] (38.82)[24]	0.05
$a^{+3}\Pi$	10.191	10.171	1.540	1734.08 (1729.79)[24]	76.82 (103.68)[24]	−1.40

The SiH_n mixture was twice skimmed before arriving in the interaction chamber (pressure of 2×10^{-7} mbar) and crossing at a right angle the monochromatized synchrotron radiation in the center of the double-imaging photoelectron/photoion spectrometer DELICIOUS3.[28] The photon resolution in the 7–10.5 eV energy range was about $\delta\lambda$ = 2.16 Å corresponding to δE varying from 9 to 19 meV over the whole domain. The photoions and the photoelectrons were extracted by an 88.7 V/cm DC field in opposite directions and detected by two VMI (Velocity Map Imaging) detectors.

The signals acquired along the measurement were corrected by the photon flux evolution independently recorded on a Si photodiode (AXUV, IRD). The coincidence scheme leads to ion-mass filtered photoelectron images that were then Abel inverted to extract the mass-selected photoelectron spectra, recorded in our case for the SiH radical. The SiH signal was thus recorded as a function of electron kinetic energy and photon energy leading to the 2D-matrix displayed in Fig. 2(a). To facilitate integration along the kinetic energy scale of a given ionic state and improve the signal-to-noise ratio of the final photoelectron spectrum, treatment of the photoelectron matrix was then performed so that the constant ionic state lines initially diagonal became vertical. The x axis values of the rotated photoelectron matrix correspond to the difference between photon energy and photoelectron kinetic energy [see Fig. 2(b)]. From the rotated matrix, the slow photoelectron spectrum (SPES) was extracted by integrating the signal over a narrow kinetic energy range (0–10 meV), following the previous methodology.[29,30] The total SPES resolution was measured at 10 meV at 7.9 eV by using the Si atom ionization transitions. The calibration of energy scale was achieved with an absolute accuracy of ±3 meV by using the Si and He third-order ionization transitions. Note that the 88.7 V/cm extraction field leads to a field-induced downshift of the *IE*s of ~7 meV. After correction by this shift, the absolute accuracy on each ionization threshold retrieved from the spectrum was estimated to be ±5 meV.

In addition, the spectra displayed in this paper have been treated to remove any contributions from the ^{29}Si isotope that appears at the same mass as ^{28}SiH. They, thus, correspond to the ^{28}SiH dominant isotopolog. To perform this correction, in energy ranges where the ^{28}SiH ion signal is negligible compared with that of ^{29}Si, we have checked that our sample is representative of the ^{29}Si-isotope natural abundance (5.1% with respect to ^{28}Si). 5.1% of the spectrum obtained on the ^{28}Si mass channel was thus subtracted from the signal of the ^{28}SiH mass channel. The absence of the strong Si autoionization resonance in the ^{28}SiH total ion yield validates our correction procedure.

III. RESULTS AND DISCUSSION

A. Photoelectron spectrum

Figure 3 displays the SPES spectrum obtained from integration of the mass-selected photoelectron signal of Fig. 2(b) over the

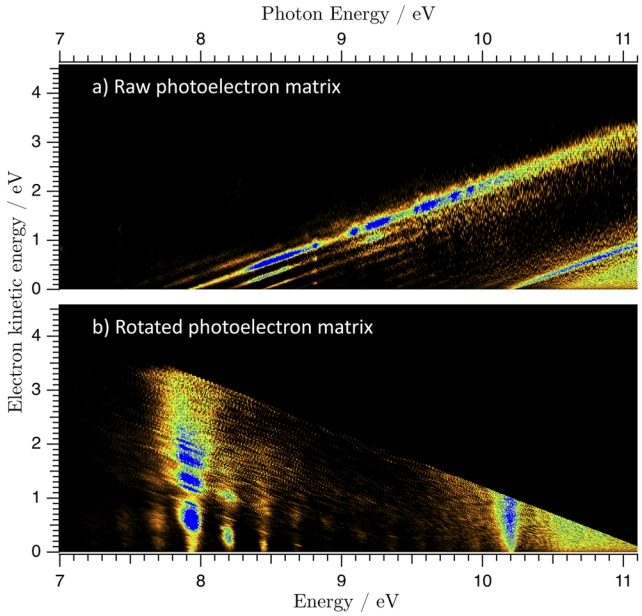

FIG. 2. Panel (a) Raw photoelectron matrix corresponding to m/z = 29; panel (b) Rotated matrix so that constant ionic state lines are now vertical and the horizontal axis values correspond to the difference (photon energy–photoelectron kinetic energy) in eV. The colormap has been adjusted to saturate autoionization lines (which appear now as diagonals) to show low intensity signals.

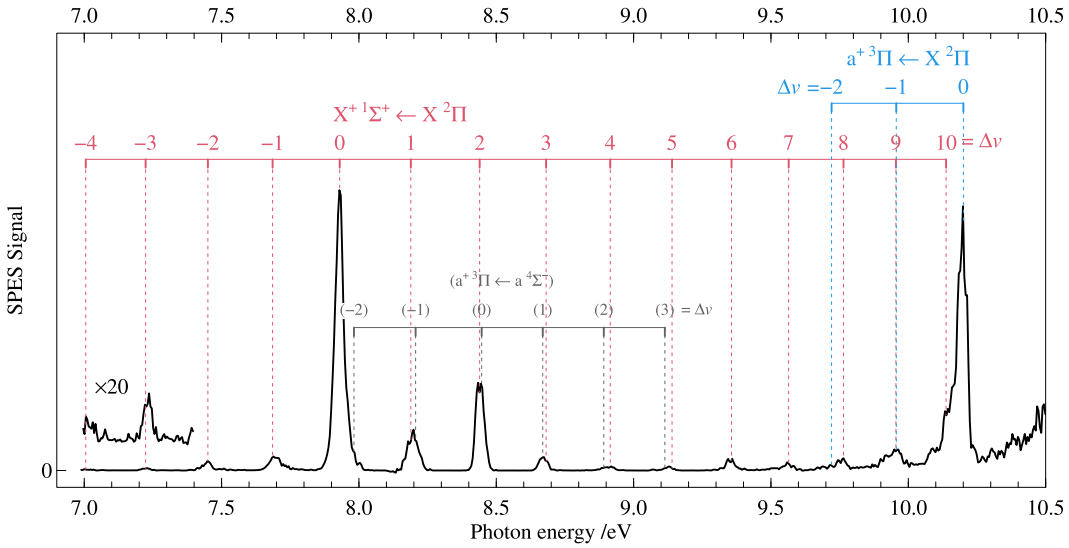

FIG. 3. Slow photoelectron spectrum of the SiH radical between 7.0 and 10.5 eV. The combs displayed as dotted lines are derived from our calculated vibrational parameters in Table I. Their absolute positions have been adjusted with the help of our calculations and the experimental spectrum. The three origin bands are assumed to be at around 7.93, 8.46, and 10.20 eV. The red and blue combs mark the observed Δv bands for the $X^{+1}\Sigma^+ \leftarrow X^2\Pi$ and $a^{+3}\Pi \leftarrow X^2\Pi$ photoionization transitions, respectively. The gray comb and the labels between brackets locate the calculated energies of the $a^{+3}\Pi \leftarrow a^4\Sigma^-$ transitions (probably unobserved here, see assignment discussion detailed in the text).

0–10 meV kinetic energy range. Photoionizing transitions involving the ground ($X^{+1}\Sigma^+$) and the first excited ($a^{+3}\Pi$) electronic states of SiH^+ are unambiguously observed. The most intense bands located at around 7.93 and 10.2 eV are assigned to the origin bands of the $X^{+1}\Sigma^+ \leftarrow X^2\Pi$ and the $a^{+3}\Pi \leftarrow X^2\Pi$ transitions, respectively. Several weaker bands are observed from either side of these two intense bands, corresponding to vibrational progressions and assigned by their Δv value. Above 10.3 eV, the photoelectron spectrum presents an onset due to contribution from the $SiH_3 \rightarrow SiH^+ + H_2 + e^-$ dissociative ionization channel. This point will be discussed in a forthcoming paper dedicated to SiH_3.

Each Δv ($= v^+ - v$) band is, in fact, the overlap of transitions from the different vibrational states v populated in the electronic ground state corresponding to a group of sequence bands. For instance, the $\Delta v = 0$ band of the $X^{+1}\Sigma^+ \leftarrow X^2\Pi$ transition is the superposition of the $X^{+1}\Sigma^+$ ($v^+ = v$) $\leftarrow X^2\Pi$ (v) transitions with different v values from 0 to 4. Indeed, observation of the $\Delta v = -4$ band around 7 eV (see the magnified part of the spectrum to the left of Fig. 3) demonstrates that the vibrational states of the neutral SiH ground state are populated up to at least $v = 4$ in the radical source. At first glance, the intensity of the $\Delta v = +2$ band of the $X^{+1}\Sigma^+ \leftarrow X^2\Pi$ transition is too intense with respect to the overall vibrational progression, which could be the signature of another photoionizing transition involving the $a^4\Sigma^-$ metastable state of neutral SiH: $a^{+3}\Pi \leftarrow a^4\Sigma^-$. Indeed, from the electronic energy of the $a^4\Sigma^-$ state with respect to the ground state of the neutral SiH (see Fig. 1), the $a^{+3}\Pi \leftarrow a^4\Sigma^-$ transition should occur at about 8.46 eV[17,21,31] and its potential vibrational progression would also partially coincide with the vibrational progression of the $X^{+1}\Sigma^+ \leftarrow X^2\Pi$ transition (see the gray comb in Fig. 3). In addition, the successive exothermic H-abstraction reactions needed for the production of the SiH radical,[17]

$$SiH_4(X\ ^1A_1) + F(^2P) \rightarrow SiH_3(X\ ^2A_1) + HF(X\ ^1\Sigma^+) \quad (\Delta H_r = -1.9\ \text{eV}), \tag{1}$$

$$SiH_3(X\ ^2A_1) + F(^2P) \rightarrow SiH_2(X\ ^1A_1) + HF(X\ ^1\Sigma^+) \quad (\Delta H_r = -2.1\ \text{eV}), \tag{2}$$

$$SiH_2(X\ ^1A_1) + F(^2P) \rightarrow SiH(X\ ^2\Pi) + HF(X\ ^1\Sigma^+) \quad (\Delta H_r = -2.1\ \text{eV}), \tag{3}$$

lead to a total excess energy larger than 6 eV distributed as kinetic and internal energies between the HF and SiH_n fragments. As the $a^4\Sigma^-$ state of SiH is located 1.75 eV[21] above the ground state, the population of this state is energetically possible. Meanwhile, this excess energy of the reaction system can also be the source of high vibrational temperature, explaining the population up to $v = 4$ in the neutral electronic ground state. However, it should be noted that in similar reactions of hydrogen atom abstraction by fluorine,[32,33] the excess energy of these reactions was found mainly as vibrational energy in HF and, therefore, one expects relatively little internal energy in SiH, although its production reactions are highly exothermic.

To figure out whether bands involving the metastable state of neutral SiH ($a^4\Sigma^-$) are observed, Franck–Condon (FC) calculations have been performed independently for all three photoionizing transitions ($X^{+1}\Sigma^+ \leftarrow X^2\Pi$, $a^{+3}\Pi \leftarrow X^2\Pi$, and $a^{+3}\Pi \leftarrow a^4\Sigma^-$), neglecting

the rotational structure, and the resulting simulated spectra are displayed in Fig. 4. Note that, in this figure, to compare the calculations with the experimental spectrum, we had to lower the energy scale of our calculated spectrum by 7 meV to account for the Stark-shift induced by the extraction electric field (see Sec. II B). The vibrational temperature was manually adjusted at 2500 K based on the following procedure. Since the experimental spectrum could not be well described by FC calculations, the vibrational temperature could not be adjusted with respect to the hot band intensities. We, thus, used the fact that the ω_e vibrational frequencies are quite different between the X and a^+ states (see Table I), which implies a very asymmetric profile of the corresponding origin band of the $a^{+3}\Pi \leftarrow X^2\Pi$ photoionizing transition located around 10.2 eV [see panel (c) of Fig. 4]. By adjusting the vibrational temperature, we succeeded in reproducing this shape satisfactorily, and we kept this temperature for the other transitions displayed in Figs. 4(b) and 4(d) to be consistent.

These calculations indicate that the FC factors corresponding to these three $\Delta v = 0$ transitions are close to 1 and the spectrum should exhibit almost exclusively the origin bands for all three transitions [see panels (b)–(d) of Fig. 4]. This can be easily predicted from Fig. 1 that depicts the potential energy curves calculated in this paper for the two lowest electronic states of the neutral and the cationic species. In this figure, it is obvious that the equilibrium Si–H bond lengths of these four states are very close and all the potential energy curves are quite parallel around their minima.

On the other hand, as earlier pointed out by Berkowitz *et al.*,[17] it is clear that strong autoionizations exist in the energy region of $\Delta v = 2$ band of the $X^{+1}\Sigma^+ \leftarrow X^2\Pi$ photoionizing transition (≈8.45 eV). To investigate the effect of this process on the treated signal, as shown in Fig. 5, we plot two slow photoelectron spectra

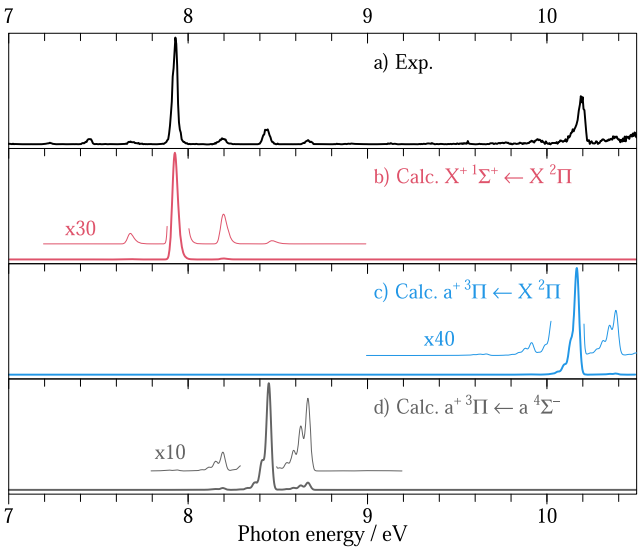

FIG. 4. Comparison between the experimental SPES [panel (a)] and the calculated spectra (T_{vib} = 2500 K, *FWHM* = 30 meV) for the $X^{+1}\Sigma^+ \leftarrow X^2\Pi$ [in red, panel (b)], $a^{+3}\Pi \leftarrow X^2\Pi$ [in blue, panel (c)], and $a^{+3}\Pi \leftarrow a\,^4\Sigma^-$ [in gray, panel (d)] photoionizing transitions. In panels (b)–(d), a zoomed-in view of the calculated spectrum is shown to better observe the vibrational progressions.

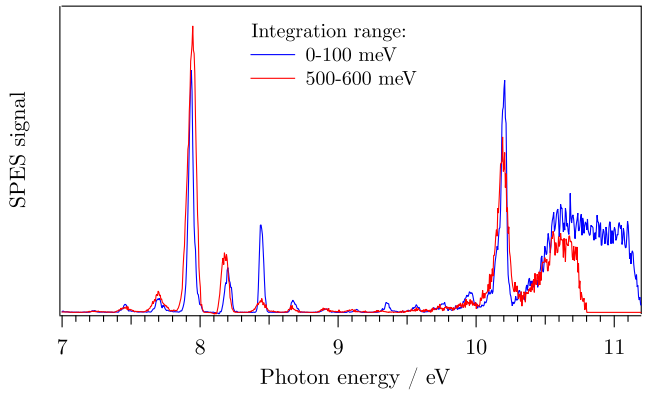

FIG. 5. SPES spectra extracted from the rotated matrix of Fig. 2(b) for two different electron kinetic energy ranges (0–100 meV in blue, 500–600 meV in red) show strong autoionization effects in the vibrational branching ratios for threshold photoelectrons. Note that the broad signal appearing above 10.3 eV corresponds to contribution from dissociative ionization of the SiH_3 radical also produced in our experiment.

extracted from the rotated matrix by integrating over two different kinetic energy ranges, 0–100 and 500–600 meV. They are shown as blue and red curves, respectively. For direct ionization to an ionic state, the contribution to the SPES will remain the same, assuming that the partial cross-section does not change much near the threshold. For autoionization, however, since autoionizing states appear at a given photon energy and not along the constant ionic state lines, their contribution to the SPES will be dramatically different for different integration intervals.

From the two spectra displayed in Fig. 5, it is noted, indeed, that autoionization processes affect differently both spectra, and this is particularly true for the $\Delta v = 2$ band located around 8.45 eV. For threshold electrons (blue spectrum), the behavior of this vibrational band is clearly non-FC,[34] whereas for faster photoelectrons (red spectrum), outside the influence of autoionization, the intensity of this transition is more consistent with our calculated FC factors (see Fig. 4). If direct ionization of the metastable state ($a^{+3}\Pi \leftarrow a^4\Sigma^-$ photoionizing transition) dominated at the photon energy of the $\Delta v = 2$ band, we would expect its relative intensity with respect to the other bands not to depend so dramatically on electron kinetic energy, and a "non-FC behavior" should be observed at all electron kinetic energies due to the addition of the photoionizing transition from the neutral metastable state. From the observed SPES difference, the contribution of the photoionizing transition from the neutral $a\,^4\Sigma^-$ metastable state appears negligible.

To extract the ionization energies from our experimental spectrum, we performed a simple simulation of the $X^{+1}\Sigma^+ \leftarrow X^2\Pi$ transition neglecting the spin–orbit coupling and the rotational structure. Only the vibrational structures of SiH and SiH^+ were then considered by using the experimental vibrational wavenumbers from Refs. 35 and 36. Note that the experimental spectral resolution is not high enough to perform a more sophisticated simulation including the rotational and the spin-orbit structures, even if the corresponding molecular constants are known.[36] As about ten Δv bands are observed for the $X^+ \leftarrow X$ photoionizing transition and at least four vibrational levels are populated in the ground state ($\Delta v = -3$ is

clearly observed), such a model would imply the manual fit of too many parameters such as the vibrational, rotational, and spin temperatures that are not necessarily thermalized in our experiment, as well as the rotational branch intensities and the Franck–Condon factors (affected by autoionization processes) to model the different Δv band intensities. To reduce drastically this number of parameters, we imposed that the FC factors for a given Δv band be the same for the corresponding transitions starting from each v level, which is usually the case for the transitions starting from the first vibrational states. For the $\Delta v = 0$ band, we fixed $FC(v = 0 \rightarrow v^+ = 0) = FC(v = 1 \rightarrow v^+ = 1) = FC(v = 2 \rightarrow v^+ = 2) = \cdots = 1$ instead of our calculated values (0.992, 0.975, and 0.958, respectively); for the $\Delta v = +1$ band, $FC(v = 0 \rightarrow v^+ = 1) = FC(v = 1 \rightarrow v^+ = 2) = FC(v = 2 \rightarrow v^+ = 3) = \cdots = 0.05$ instead of 0.008, 0.015, 0.022, etc.; for the $\Delta v = +2$ band, $FC(v = 0 \rightarrow v^+ = 2) = FC(v = 1 \rightarrow v^+ = 3) = FC(v = 2 \rightarrow v^+ = 4) = \cdots = 0.12$ instead of 0.0006, 0.0019, 0.0037, etc.. Here, the ionization energies and band intensities (i.e., the FC factors) were the only manually adjusted parameters and the modeled stick spectrum was convolved with a Gaussian line shape with a full width at half maximum (FWHM) of 30 meV to mimic the rotational and spin–orbit structures. The vibrational temperature was kept at 2500 K, similar to the simulation displayed in Fig. 4.

The obtained result for the $X^{+1}\Sigma^+ \leftarrow X^2\Pi$ transition is depicted in Fig. 6. Note that the differences between this latter simulation and the FC simulation reported in panel (b) of Fig. 4 are the use of experimental vibrational constants from Ref. 35, which better reproduce the sequence band positions, and the use of manually adjusted intensity factors for each Δv band (keeping the same intensity factor for given sequence bands), which facilitates the band shape comparisons. The goal here was to take into account each component of each Δv band (−4 up to +4) to reproduce as well as possible each band shape (for instance, $\Delta v = +2$ that is much narrower than $\Delta v = -1$). The fact that we correctly reproduce the different shapes of the vibrational bands allows us to limit the effect of the autoionization on the determination of the adiabatic ionization energy, even without determining the vibrational distribution of SiH in our experiment.

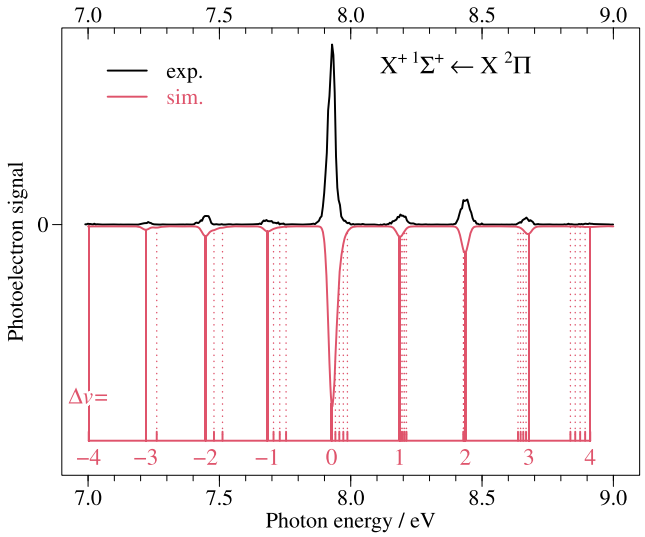

FIG. 6. Experimental SPES of SiH in the vicinity of the $X^{+1}\Sigma^+ \leftarrow X^2\Pi$ transition (in black) and calculated spectrum (in red). The red comb locates the energies of each $\Delta v(= v^+ - v)$ band involving one populated v level of the SiH electronic ground state, with the smallest v value of a given group of sequence bands displayed in solid vertical line.

TABLE II. Experimental adiabatic photoionization energies IE_{ad} of SiH in eV, measured in this paper and compared with the results of Ref. 17.

State	This work	Reference 17
$X^{+1}\Sigma^+ \leftarrow X^2\Pi$	7.934(5)	7.91(1)
$a^{+3}\Pi \leftarrow X^2\Pi$	10.205(5)	10.21(1)

The positions of the $X^{+1}\Sigma^+$ ($v^+ = 0$) ← $X^2\Pi$ ($v = 0$) and $a^{+3}\Pi$ ($v^+ = 0$) ← $X^2\Pi$ ($v = 0$) transitions derived with the procedure described in the previous paragraph correspond to the adiabatic ionization energies (IE_{ad}) toward these two cationic states. These values, after field-induced shift corrections, are reported in Table II. Note that these ionization energies are given with 1σ (standard deviation) error bars and have been derived neglecting the spin–orbit (SO) coupling that occurs in the neutral ground state with a SO coupling constant[36] $A_{SO} = 142.83\ cm^{-1}$ and possible asymmetric rotational envelopes. In Tables I and II, the calculated and experimental results obtained in this work are compared with values from the literature. The agreements are excellent. Our measured transition energies confirm the ones obtained by Berkowitz *et al.*[17] by photoionization mass spectrometry and the calculation of Rosmus and Meyer.[19]

Similar to the work of Berkowitz *et al.*,[17] our experimental *IE* value can be used to derive the dissociation energy $D_0(SiH)$ of the silylidyne radical using the following equation:

$$IE(SiH) + D_0(SiH^+) = D_0(SiH) + IE(Si).$$

With the known values of $IE(Si) = 8.15166(3)$ eV,[37] $D_0(SiH^+) = 3.22(3)$ eV,[38] and our measurement, we obtain $D_0(SiH) = 3.00(3)$ eV, which agrees with the value obtained by Berkowitz *et al.* [2.98(3) eV] and the limit given by Huber and Herzberg [$D_0(SiH) \leq 3.060$ eV].[35]

The calculated and experimental energy differences between the two lowest cationic states [$\Delta E_{X^+-a^+} = T_0(a^+) - T_0(X^+)$] are 2.24 and 2.271(5) eV, respectively. These results are in good agreement with the calculated ΔE values of Sannigrahi *et al.* (2.31 eV, corrected from the ZPE).[31] The experimental ΔE value obtained by Berkowitz *et al.*[17] is of 2.30 ± 0.01 eV, indirectly inferred from the Rydberg series converging to a^+ (see Sec. III B).

B. Photoion yield

The mass-selected SiH^+ photoion yield recorded in this paper is displayed in Fig. 7, and a tentative analysis is proposed in this section based on the previous work of Berkowitz *et al.*[17]

The configuration of the electronic ground state of the SiH united-atom system[39] is $[\cdots](3s\sigma)^2(3p\sigma)^2(3p\pi)^1$. Ionization toward the $X^{+1}\Sigma^+$ and $a^{+3}\Pi$ cationic states involves in both cases the removal of a "p-like" electron ($3p\pi$ and $3p\sigma$, respectively). This

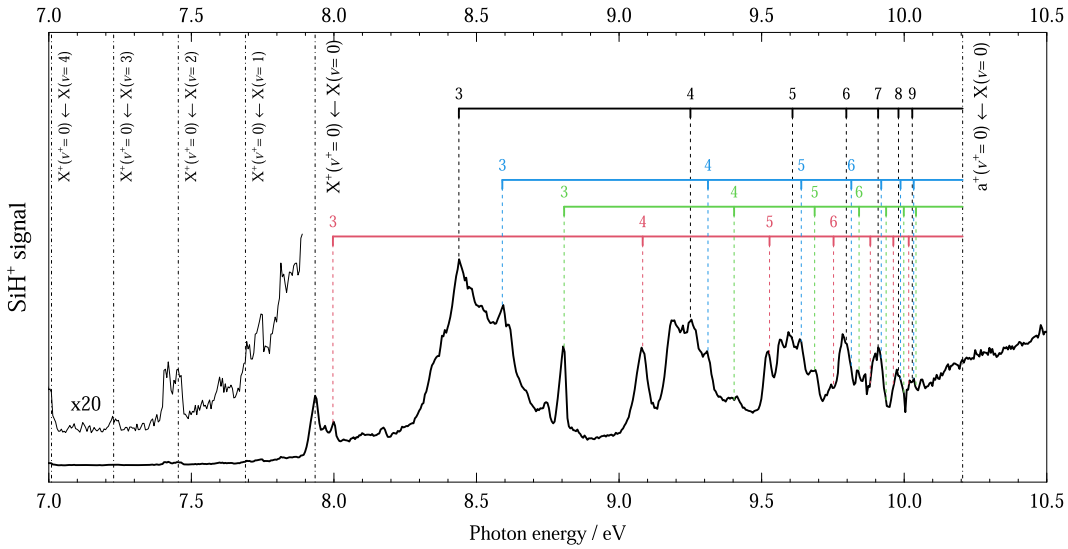

FIG. 7. Mass-selected ion yield of the SiH radical. The labels located by combs correspond to the assignments of the Rydberg series of neutral species observed by autoionization. The black, blue, green, and red combs correspond to the transitions from $X^2\Pi$ ($v = 0$) to the Rydberg series converging to the $a^{+3}\Pi$ ($v^+ = 0$) state with quantum defect δ equal to 0.225, 0.097, −0.120, and 0.518. The gray dashed vertical lines locate ionization thresholds originating from different vibrational levels of neutral SiH.

leads to the expectation of only s and d neutral Rydberg series, whose member energies follow the Rydberg formula

$$E_{\mathrm{Ry}} = IE - \frac{Ry}{(n^*)^2}, \tag{4}$$

with Ry being the Rydberg constant of SiH (Ry = 13.60544 eV), n^* being the effective quantum number such that $n^* = n - \delta$, and δ being the quantum defect.

In their paper, Berkowitz *et al.*[17] identified two Rydberg series converging to the $a^{+3}\Pi$ cationic state. The first one is composed of broad features and is assigned to a "d-" or "s-like" Rydberg series. A second one is suspected to be a "p-like" series allowed through l-spoiling of the non-spherical molecular potential.[17]

In Fig. 7, four combs are displayed corresponding to fitted Rydberg series converging to the a^+ cationic state using Eq. (4), the adiabatic ionization energy derived from the photoelectron spectrum [10.205(5) eV], and four different quantum defects [0.225 (in black), 0.518 (in red), 0.097 (in blue), and −0.120 (in green)]. The labeling of the principal quantum number is uncertain and has been arbitrarily started at $n = 3$ for each series. This means that the quantum defect values given in this paper are given modulo an integer (e.g., −0.120 might correspond to a quantum defect of 0.88 or 1.88, ...). Note that for hydrocarbon molecules, quantum defects associated with s, p, and d series have typical δ values close to 1, 0.5, and 0, respectively (see, for instance, Table 3 of Ref. 40). For molecules with heavier atoms, these values can be significantly higher, with quantum defects close to 2 for s series, for instance, for the S_2 molecule (see Table 2 in Ref. 41). In this paper, it is not possible to distinguish between a "s" or "d" character of the corresponding states since the principal quantum number value is not unambiguously assigned (note that Berkowitz *et al.* did not conclude either on this character). What we can predict from the electronic configuration of the neutral species is that the expected Rydberg series converging to the a^+ state are s or d series since they correspond to the removal of an electron from the 3pσ orbital. In our experiment, the SiH is produced in several vibrational levels (see Sec. III A), and for each series, several sequence bands exist [i.e., Rydberg states converging toward $a^{+3}\Pi(v^+ = v)$ and reached from $X^2\Pi(v)$ state with v = 0, 1, 2, ...]. For the sake of clarity, only the Rydberg transitions from $v = 0$ are reported.

The Rydberg series associated with the red and black combs corresponds to the ones reported by Berkowitz *et al.*,[17] who derived n^* values rather than a constant δ value for a series. The blue and green combs, not observed by Berkowitz *et al.*,[17] are tentative new assignments. These two new series would correspond to "s-" or "d-like" series in view of their quantum defect values (0.097 and −0.120). Nevertheless, it is not possible to distinguish between the "s" or "d" character of such series, since the principal quantum number values are not unambiguously assigned.

All the strong features located by the combs in Fig. 7 are due to electronic autoionization as was found in our previous study on the CH radical.[30]

It should be noted that the $n = 3$ state of the δ = 0.225 Rydberg series coincides with the $v^+ = 2$ vibrational level of $X^{+1}\Sigma^+$ cationic state, leading to a strong autoionization-at-threshold structure (i.e., releasing a photoelectron without kinetic energy), which could explain the intense band in the SPES spectrum corresponding to the $\Delta v = 2$ band of the $X^{+1}\Sigma^+$ (v^+) ← $X^2\Pi$ (v) transitions.

One sharp feature in the ion yield matching the ionization energy ($X^+ \leftarrow X$ at 7.934 eV) remains unassigned (either in this work or in the Berkowitz *et al.* paper; see Ref. 17). This feature seems to

be observed as weak "hot bands" below the first ionization energy due to population of excited vibrational states in the neutral ground state (see the magnified portion of the spectrum in Fig. 7). Indeed, as shown in Fig. 7, when reporting the ionization thresholds corresponding to transitions involving vibrationally excited levels in the neutral ground state toward the vibronic ground state of the cation ($v^+ = 0$), these energies match weaker peaks observed in the ion yield that we assign to hot bands. The remaining structures in this region are most probably due to vibrational autoionization processes as in the case of the CH radical.[30]

IV. CONCLUSIONS AND PERSPECTIVES

In this paper, we measured for the first time the threshold photoelectron spectrum of the SiH radical by coupling a flow-tube reactor and a double-imaging photoelectron/photoion spectrometer. The adiabatic ionization energies for the electronic ground state $X^{+1}\Sigma^+$ and the first excited electronic state $a^{+3}\Pi$ have been determined, in good agreement with our calculated values as well as the previous study of Berkowitz *et al.*,[17] based on photoionization mass spectrometry with an improved accuracy.

Investigations at higher spectral resolution, using laser-based experiment such as pulsed-field-ionization zero-kinetic energy photoelectron spectroscopy, would be of great interest to resolve the fine structure of the above-mentioned ionizing transitions (including the rotational and spin–orbit structures) to determine more precisely the ionization energies.

The strong autoionization features observed in the SiH^+ ion yield were also discussed based on the previous work of Berkowitz *et al.*,[17] and a tentative assignment of additional Rydberg series was proposed. Similar strong autoionization processes were also observed in our previous work on CH radical with the same experiment.[30] These two systems (CH and SiH) are benchmark systems to study autoionization processes, and our experimental ion yields might stimulate new theoretical studies.

Finally, during our experiment, the radical source conditions allowed the production of other Si-bearing radicals, such as SiH_3, SiH_2, Si_2, Si_2H, Si_3, as well as products with fluorine atoms (SiF, for instance). Thanks to the mass-selectivity of the double-imaging spectrometer, all photoelectron and photoion signals have been recorded simultaneously, and analysis of these spectra will be published in forthcoming papers. In particular, the dissociative ionization channel of SiH_3 appearing above 10.3 eV ($SiH_3 \rightarrow SiH^+ + H_2 + e^-$) will be discussed with the help of the present SiH^+ ion yield.

SUPPLEMENTARY MATERIAL

See the supplementary material for the experimental dataset of the photoelectron spectrum reported in Fig. 3 and for the photoion yield reported in Fig. 7.

ACKNOWLEDGMENTS

This work was performed on the DESIRS Beamline at SOLEIL synchrotron under Proposal No. 20200996. We are grateful to the whole staff of SOLEIL for running the facility. Ning L. Chen acknowledges the support from the Paris Ile-de-France Region (DIM ACAV+) for her Ph.D. grant.

This work has also received financial support from the French "Agence Nationale de la Recherche" (ANR) under Grant No. ANR-12-BS08-0020-02 (Project SYNCHROKIN). This work was supported by the Programme National "Physique et Chimie du Milieu Interstellaire" (PCMI) of CNRS/INSU with INC/INP cofunded by CEA and CNES.

AUTHOR DECLARATIONS

Conflict of Interest

The authors have no conflicts to disclose.

Author Contributions

Ning L. Chen: Conceptualization (equal); Investigation (equal); Writing – original draft (equal). **Bérenger Gans:** Formal analysis (equal); Investigation (equal); Supervision (equal); Writing – review & editing (equal). **Sebastian Hartweg:** Formal analysis (equal); Investigation (equal). **Gustavo A. Garcia:** Formal analysis (equal); Investigation (equal); Resources (equal); Validation (equal). **Séverine Boyé-Péronne:** Funding acquisition (equal); Investigation (equal); Supervision (equal); Writing – original draft (equal); Writing – review & editing (equal). **Jean-Christophe Loison:** Investigation (equal); Methodology (lead); Writing – original draft (equal).

DATA AVAILABILITY

The data that support the findings of this study are available within the article and its supplementary material.

REFERENCES

[1] E. Herbst, T. J. Millar, S. Wlodek, and D. K. Bohme, "The chemistry of silicon in dense interstellar clouds," Astron. Astrophys. **222**, 205–210 (1989).
[2] K. Lodders, "Solar system abundances and condensation temperatures of the elements," Astrophys. J. **591**, 1220–1247 (2003).
[3] B. D. Savage and K. R. Sembach, "Interstellar abundances from absorption-line observations with the *Hubble Space Telescope*," Annu. Rev. Astron. Astrophys. **34**, 279–329 (1996).
[4] E. B. Jenkins, "A unified representation of gas-phase element depletions in the interstellar medium," Astrophys. J. **700**, 1299–1348 (2009); arXiv:0905.3173.
[5] J. Cernicharo, C. A. Gottlieb, M. Guélin, P. Thaddeus, and J. M. Vrtilek, "Astronomical and laboratory detection of the SiC radical," Astrophys. J. **341**, L25–L28 (1989).
[6] D. M. Goldhaber and A. L. Betz, "Silane in IRC +10216," Astrophys. J. **279**, L55–L58 (1984).
[7] L. M. Ziurys, P. Friberg, and W. M. Irvine, "Interstellar SiO as a tracer of high-temperature chemistry," Astrophys. J. **343**, 201 (1989).
[8] B. E. Turner, H. H. Lee, and E. Herbst, "The physics and chemistry of small translucent molecular clouds. IX. Acetylenic chemistry," Astrophys. J., Suppl. Ser. **115**, 91–118 (1998).
[9] R. Lucas and H. Liszt, "SiO in diffuse, translucent and 'spiral-arm' clouds," Astron. Astrophys. **355**, 327–332 (2000).
[10] L. M. Ziurys, D. P. Clemens, R. J. Saykally, M. Colvin, and H. F. Schaefer, "A search for interstellar silicon nitride," Astrophys. J. **281**, 219–224 (1984).
[11] P. Schilke, S. Leurini, K. M. Menten, and J. Alcolea, "Interstellar SiN," Astron. Astrophys. **412**, L15–L18 (2003).

[12]L. Podio, C. Codella, B. Lefloch, N. Balucani, C. Ceccarelli, R. Bachiller, M. Benedettini, J. Cernicharo, N. Faginas-Lago, F. Fontani, A. Gusdorf, and M. Rosi, "Silicon-bearing molecules in the shock L1157-B1: First detection of SiS around a Sun-like protostar," Mon. Not. R. Astron. Soc.: Lett. **470**, L16–L20 (2017); arXiv:1705.01794.
[13]M. Guélin, S. Muller, J. Cernicharo, A. Apponi, M. McCarthy, C. Gottlieb, and P. Thaddeus, "Astronomical detection of the free radical SiCN," Astron. Astrophys. **363**, L9–L12 (2000).
[14]P. Schilke, D. J. Benford, T. R. Hunter, D. C. Lis, and T. G. Phillips, "A line survey of Orion-KL from 607 to 725 GHz," Astrophys. J., Suppl. Ser. **132**, 281–364 (2001).
[15]A. A. de Almeida and P. D. Singh, "Predictions on finding the SiH^+ and SiH in instestellar space," Astrophys. Space Sci. **56**, 415–419 (1978).
[16]A. G. G. M. Tielens, "Chemical processes," in *The Physics and Chemistry of the Interstellar Medium* (Cambridge University Press, 2005), pp. 85–116.
[17]J. Berkowitz, J. P. Greene, H. Cho, and B. Ruščić, "Photoionization mass spectrometric studies of SiH_n (n = 1–4)," J. Chem. Phys. **86**, 1235–1248 (1987).
[18]J. A. Pople and L. A. Curtiss, "Theoretical thermochemistry. 3. A modified procedure for ionization energies of AHn species," J. Phys. Chem. **91**, 3637–3639 (1987).
[19]P. Rosmus and W. Meyer, "PNO-CI and CEPA studies of electron correlation effects. IV. Ionization energies of the first and second row diatomic hydrides and the spectroscopic constants of their ions," J. Chem. Phys. **66**, 13–19 (1977).
[20]H.-J. Werner, P. J. Knowles, G. Knizia, F. R. Manby, M. Schütz, P. Celani, T. Korona, R. Lindh, A. Mitrushenkov, G. Rauhut, K. R. Shamasundar, T. B. Adler, R. D. Amos, A. Bernhardsson, A. Berning, D. L. Cooper, M. J. O. Deegan, A. J. Dobbyn, F. Eckert, E. Goll, C. Hampel, A. Hesselmann, G. Hetzer, T. Hrenar, G. Jansen, C. Köppl, Y. Liu, A. W. Lloyd, R. A. Mata, A. J. May, S. J. McNicholas, W. Meyer, M. E. Mura, A. Nicklass, D. P. O'Neill, P. Palmieri, D. Peng, K. Pflüger, R. Pitzer, M. Reiher, T. Shiozaki, H. Stoll, A. J. Stone, R. Tarroni, T. Thorsteinsson, and M. Wang, MOLPRO, version 2015.1, a package of *ab initio* programs, 2015.
[21]Y.-G. Zhang, G. Dou, J.-X. Qi, and J. Cui, "*Ab inito* study on the electronic structure and laser cooling of SiH," Comput. Theor. Chem. **1134**, 8–14 (2018).
[22]C. M. Western, "PGOPHER: A program for simulating rotational, vibrational and electronic spectra," J. Quant. Spectrosc. Radiat. Transfer **186**, 221–242 (2017).
[23]S. Gozem and A. I. Krylov, "The *ezSpectra* suite: An easy-to-use toolkit for spectroscopy modeling," Wiley Interdiscip. Rev.: Comput. Mol. Sci. **12**, e1546 (2022).
[24]D. M. Hirst, "Ab initio potential energy curves for the X $^1\Sigma^+$, A $^1\Pi$, a $^3\Pi$ and $^3\Sigma^+$ states of SiH^+," Chem. Phys. Lett. **128**, 504–506 (1986).
[25]L. Nahon, N. De Oliveira, G. A. Garcia, J.-F. Gil, B. Pilette, O. Marcouillé, B. Lagarde, and F. Polack, "DESIRS: A state-of-the-art VUV beamline featuring high resolution and variable polarization for spectroscopy and dichroism at SOLEIL," J. Synchrotron Radiat. **19**, 508–520 (2012).
[26]X. Tang, G. A. Garcia, J.-F. Gil, and L. Nahon, "Vacuum upgrade and enhanced performances of the double imaging electron/ion coincidence end-station at the vacuum ultraviolet beamline DESIRS," Rev. Sci. Instrum. **86**, 123108 (2015).
[27]G. A. Garcia, B. Gans, X. Tang, M. Ward, S. Batut, L. Nahon, C. Fittschen, and J.-C. Loison, "Threshold photoelectron spectroscopy of the imidogen radical," J. Electron Spectrosc. Relat. Phenom. **203**, 25–30 (2015).
[28]G. A. Garcia, B. K. Cunha de Miranda, M. Tia, S. Daly, and L. Nahon, "DELICIOUS III: A multipurpose double imaging particle coincidence spectrometer for gas phase vacuum ultraviolet photodynamics studies," Rev. Sci. Instrum. **84**, 053112 (2013).
[29]J. C. Poully, J. P. Schermann, N. Nieuwjaer, F. Lecomte, G. Grégoire, C. Desfrançois, G. A. Garcia, L. Nahon, D. Nandi, L. Poisson, and M. Hochlaf, "Photoionization of 2-pyridone and 2-hydroxypyridine," Phys. Chem. Chem. Phys. **12**, 3566–3572 (2010).
[30]B. Gans, F. Holzmeier, J. Krüger, C. Falvo, A. Röder, A. Lopes, G. A. Garcia, C. Fittschen, J.-C. Loison, and C. Alcaraz, "Synchrotron-based valence shell photoionization of CH radical," J. Chem. Phys. **144**, 204307 (2016).
[31]A. B. Sannigrahi, R. J. Buenker, G. Hirsch, and J.-p. Gu, "Ab initio configuration interaction study of the electronic spectrum of SiH^+," Chem. Phys. Lett. **237**, 204–211 (1995).
[32]R. G. Macdonald and J. J. Sloan, "The microscopic reaction dynamics and branching ratio in the F + HCOOH and F + H_2CO reactions," Chem. Phys. **31**, 165–176 (1978).
[33]M. A. Wickramaaratchi, D. W. Setser, H. Hildebrandt, B. Kõrbitzer, and H. Heydtmann, "Evaluation of HF product distributions deduced from infrared chemiluminiscence. II. F atom reactions," Chem. Phys. **94**, 109–129 (1985).
[34]P. Terrence Murray and T. Baer, "Observation of vibrationally excited ions in Franck–Condon gaps by threshold photoelectron spectroscopy," Int. J. Mass Spectrom. Ion Phys. **30**, 165–174 (1979).
[35]K. P. Huber and G. Herzberg, *Molecular Spectra and Molecular Structure, Volume IV, Constants of Diatomic Molecules* (Van Nostrand Reinhold Company, New York, 1979).
[36]P. J. Linstrom and W. G. Mallard, *NIST Chemistry WebBook*, NIST Standard Reference Database Number 69 (National Institute of Standards and Technology, 2022).
[37]C. M. Brown, S. G. Tilford, R. Tousey, and M. L. Ginter, "Absorption spectrum of Si I between 1500 and 1900 Å," J. Opt. Soc. Am. **64**, 1665–1682 (1974).
[38]T. Carlson, J. Copley, N. Duric, N. Elander, P. Erman, M. Larsson, and M. Lyyra, "The oscillator strengths and the dissociation energy of SiH^+ as determined from time resolved precision spectroscopy," Astron. Astrophys. **83**, 238–244 (1980).
[39]G. Herzberg, *Molecular Spectra and Molecular Structure. I. Spectra of Diatomic Molecules* (Van Nostrand Reinhold, 1950), p. 323.
[40]F. Laruelle, S. Boyé-Péronne, D. Gauyacq, and J. Liévin, "Revisiting Mulliken's concepts about Rydberg states and Rydberg-valence interactions from large-scale ab initio calculations on the acetylene molecule," J. Phys. Chem. A **113**, 13210–13220 (2009).
[41]H. R. Hrodmarsson, G. A. Garcia, L. Nahon, J.-C. Loison, and B. Gans, "High resolution threshold photoelectron spectrum and autoionization processes of S_2 up to 15.0 eV," J. Mol. Spectrosc. **381**, 111533 (2021).